References

[1] L. E. Dickens *et al.*, "A mixer and solid state LO for a 60 GHz receiver," *IEEE-GMTT International Microwave Symposium*, pp. 188–190, May 19, 1971.
[2] L. T. Yuan, "A low noise broadband *Ka*-band waveguide mixer," *IEEE-GMTT International Microwave Symposium*, pp. 272–273, May 12, 1975.
[3] A. L. Lance, "Evaluate couplers fast and accurately," *Microwaves*, vol. 9, pp. 34–36, Nov. 1970.
[4] P. C. Ely, Jr., "Swept frequency techniques," *Proc. IEEE*, vol. 55, pp. 991–1002, June 1967.
[5] Hewlett Packard Application Note 183, "High frequency swept measurements," Appendix B.

Discussion of a 2-Gap Waveguide Mount

ROBERT L. EISENHART, MEMBER, IEEE

***Abstract*—An equivalent circuit is presented for a commonly used waveguide diode mount, providing the means for accurate theoretical analysis and design of components previously considered possible only by empirical means. Several applications are discussed and experimental confirmation is included for a variety of circuit configurations.**

I. Introduction

The purpose of this short paper is to discuss an equivalent circuit for a waveguide mounting structure. This circuit has a great deal of flexibility in application, providing accurate description for a variety of circuit configurations.

Basically, the circuit was developed to describe the waveguide mount shown in Fig. 1 which we will call the 2-gap post mount. This circuit has been used as a varactor-tuned Gunn oscillator mount [1] but was not fully understood. In addition, there is a biasing difficulty because a wire must be connected to midpost with a minimum disturbance of the surrounding fields. Whether or not the understanding made available through this equivalent circuit proves the mount in Fig. 1 to be very useful is not the major interest here. Through parallel research effort, additional knowledge has been gained which, when used in conjunction with the 2-gap equivalent circuit, allows application to a much wider range of waveguide configurations. An equivalence has been established between a coaxial entry on the bottom of the waveguide and a gap in the post at the bottom [2]. An obvious extension of this idea is that shown in Fig. 2, where the 2-gap equivalent circuit can be applied to any one of the three configurations shown. The power of this analysis is more readily apparent now, since Fig. 2 (b) and (c) is very commonly used. Note also that there is no restriction on the loading of the coaxial line or the two waveguide arms. Fig. 2(b) could represent a parametric amplifier, upconverter, or downconverter which has the appropriate filter in the coax line and a varactor in the gap. It could also be an IMPATT or Gunn oscillator with a sliding short for tuning in the coax, or perhaps use the coax to model an imperfect bias. One of the most common applications of Fig. 2(c) is the oscillator circuit attributed to Kurokawa [3] which recesses an IMPATT diode in one coax arm and puts a matched load in the other. Typically, there is a sliding short on one waveguide arm with the other being the output. Examples of circuits from Fig. 2(b) and (c) will be discussed in the experimental results.

II. Equivalent Circuit Development

The 2-gap equivalent circuit is based upon an extension of the single-gap development which was published in August 1971 [4]. It is therefore necessary that, in order to fully understand and use the material presented here, the reader should be familiar with [4], a detailed review of which would be repetitious. The extension in concept and circuit analysis is relatively straightforward from the single to the double gap.

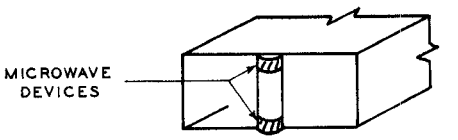

Fig. 1. 2-gap post mount.

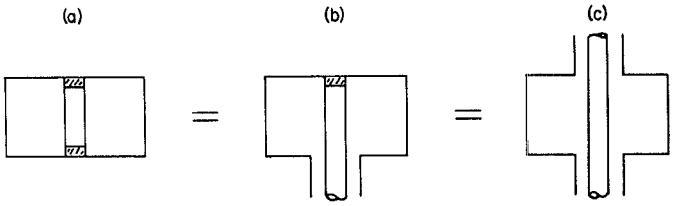

Fig. 2. Equivalent waveguide configurations for which the 2-gap circuit can be applied. (a) Double gap. (b) Gap/coax. (c) Double coax.

The concept behind the single-gap circuit is that each waveguide mode exists (a doubly infinite number) and has a loading effect on the gap driving point impedance Z_R. To accurately describe the characteristics of a particular mount configuration, it is necessary to determine the coupling mechanism between the gap terminals and each of these modes. This complex coupling action is best described by use of an equivalent circuit. Conceptually, then, the circuit only contains ideal coupling transformers between the gap and the modes, considering the mode effects as external loads. These modes are described in terms of a mode impedance which is dependent only upon the waveguide parameters and the mode indices. These mode impedances are

$$Z_H = j\frac{\eta b}{a(2-\delta_0)}\left(\frac{f}{\sqrt{f_c^2 - f^2}}\right)\left(\frac{(mb)^2}{(mb)^2 + (na)^2}\right) \tag{1a}$$

$$Z_E = -j\frac{\eta b}{a(2-\delta_0)}\left(\frac{\sqrt{f_c^2 - f^2}}{f}\right)\left(\frac{(na)^2}{(mb)^2 + (na)^2}\right) \tag{1b}$$

where

η free-space impedance = $120\pi\ \Omega$;
m,n mode indices with;
m field variation in the x direction;
n field variation in the y direction;
f_c mode cutoff frequency = $[(mc/2a)^2 + (\eta c/2b)^2]^{1/2}$;
c free-space velocity of propagation;

$$\delta_0 = \begin{cases} 1, & n = 0 \\ 0, & \text{otherwise.} \end{cases}$$

The waveguide dimensions a,b are defined in Fig. 3, along with the dimensional parameters associated with the two gaps and the post. These impedances happen to sum directly, resulting in what is called the mode pair impedance [4].

$$Z_{mn} = Z_H + Z_E. \tag{2}$$

The mode pair impedance will be resistive for propagating modes, reactive for evanescent modes, and is the terminating load at each mode port of the coupling circuit [4, fig. 5]. Fig. 4 shows this single-gap circuit but with the mode impedances combined for each value of n, where

$$Z_{Dn} = \sum_{m=1}^{M_1} Z_{mn}\kappa_{pm}^2, \qquad \text{for } n = 0,1,\cdots,N_1 \tag{3}$$

Manuscript received May 17, 1976; revised July 26, 1976.
The author is with Hughes Aircraft Company, Culver City, CA 90230.

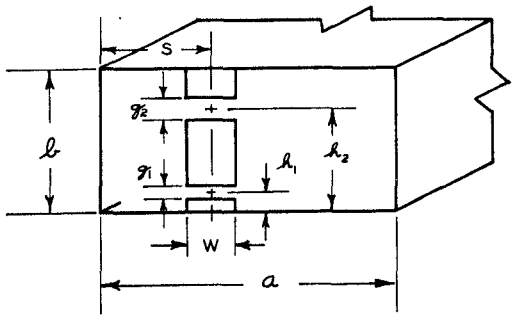

Fig. 3. Parameter description for a general 2-gap mount.

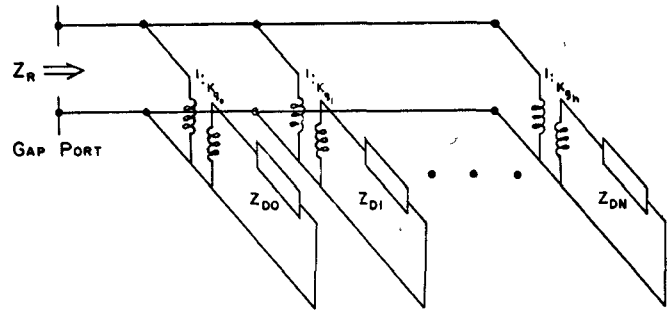

Fig. 4 Single-gap equivalent circuit.

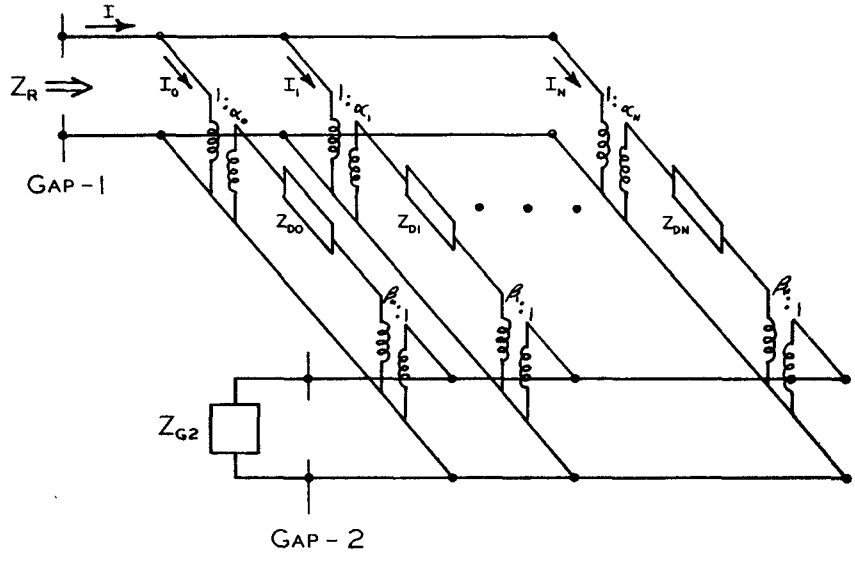

Fig 5. 2-gap equivalent circuit.

and

$$\kappa_{pm} = \sin\left(\frac{m\pi s}{a}\right)\left(\frac{\sin\dfrac{m\pi w}{2a}}{\dfrac{m\pi w}{2a}}\right).$$

Considered in this way, the extension to two gaps seems obvious and is shown in Fig. 5, where

$$\alpha_n = \cos k_y h_1 \left(\frac{\sin\phi_{1n}}{\phi_{1n}}\right) \tag{4a}$$

$$\beta_n = \cos k_y h_2 \left(\frac{\sin\phi_{2n}}{\phi_{2n}}\right) \tag{4b}$$

with

$$\phi_{in} = \frac{k_y g_i}{2}, \qquad \begin{cases} i = 1 \quad \text{or} \quad 2 \\ n = 0,1,\cdots,N_1 \end{cases}$$

$$k_y = \frac{n\pi}{b}$$

and Z_{G2} is the loading impedance of second gap. (Note: The gap coupling factor notation has been changed from κ_{gn} to α_n and β_n for the two gaps rather than adding yet another subscript and possible confusion.) This intuitive approach may not satisfy the more mathematically inclined; however, the symmetry requirements exclude any other arrangement. It was, therefore, still necessary to verify experimentally that this circuit would represent the 2-gap mount.

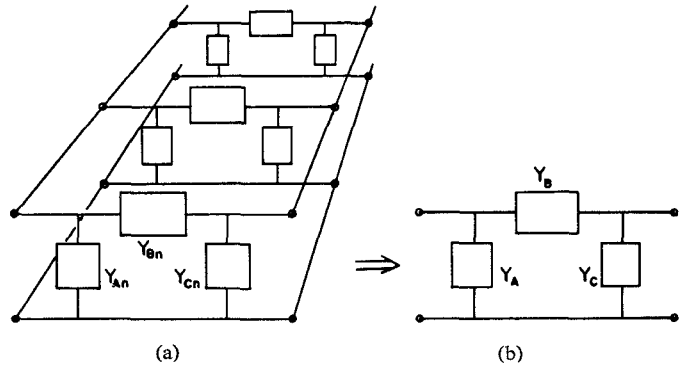

Fig. 6. π-network representation of higher order modes ($n \geq 1$). (a) Individual branches. (b) Composite network.

Before experimental verification can take place, a method must be developed to analyze this multielement circuit of variable size. (The number of modes considered depends upon the physical dimensions of the particular mount under analysis, resulting in a variable value for n.) Fortunately, a consolidation of elements is possible for the higher order modes, simplifying the equivalent circuit. Since the branches associated with each value of n are connected in parallel, it is desirable to represent each branch by a π network of elements so that these resulting branches can be combined into one equivalent π network for all $n \geq 1$ modes. Consider the π representation for each branch shown in Fig. 6(a)

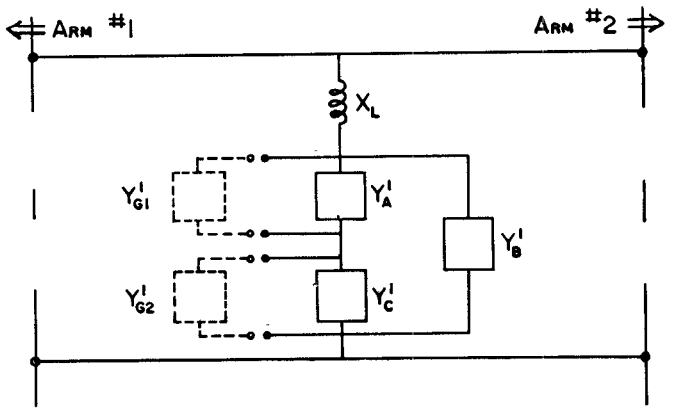

Fig. 7. Simplified 2-gap equivalent circuit.

and the consolidated circuit of Fig. 6(b). The resulting admittances come directly from the summation of the branch admittances which are standard π-network element terms, i.e., Y_{11}, Y_{12}, Y_{22} [5].

$$Y_A = \sum_{n=1}^{N_1} \frac{(\alpha_n^2 - \alpha_n\beta_n)}{Z_{Dn}} \tag{5a}$$

$$Y_B = \sum_{n=1}^{N_1} \frac{\alpha_n\beta_n}{Z_{Dn}} \tag{5b}$$

and

$$Y_C = \sum_{n=1}^{N_1} \frac{(\beta_n^2 - \alpha_n\beta_n)}{Z_{Dn}}. \tag{5c}$$

These three elements no longer represent individual mode effects but a complex combination of many modes. Therefore, it is best to leave them as admittances and not try to say they are capacitive or inductive. In fact, for higher frequencies some modes will begin to propagate, and these admittances will have real parts as well.

Consider now the first or $n = 0$ branch of Fig. 5. This is handled differently because it contains the propagating TE_{10} modes. Since their effect is dependent upon the type of loading present for the two arms of the waveguide, it is more convenient to simply consider these arms as loads through terminals to which they are attached. Then the TE_{10} loading is external to the equivalent circuit and can be controlled as desired. The rest of the modes in this branch combine to produce the "post inductance," that is, the effective shunting inductance across the waveguide which would be present if the gaps were shorted out. This is true inductance since all of the modes ($n = 0$, $m \geq 2$) contributing to the effect are inductive in nature. This first branch then appears as a parallel set of waveguide terminals in series with the post inductance. The total equivalent circuit can now be rearranged resulting in the circuit shown in Fig. 7, which is more easily related directly to the mount. This arrangement assumes that only the dominant mode is propagating. Higher order mode propagation can be handled; however, the circuit becomes more complex, or "less simplified" from the general case in Fig. 5. Since we have referred the circuit to the waveguide ports, we shall be consistent by absorbing the post coupling factor in the circuit elements as

$$Y_{G1}' = \kappa_{p1}^2/Z_{G1} \tag{6a}$$

$$Y_{G2}' = \kappa_{p1}^2/Z_{G2} \tag{6b}$$

$$Y_A' = \kappa_{p1}^2 Y_A \tag{6c}$$

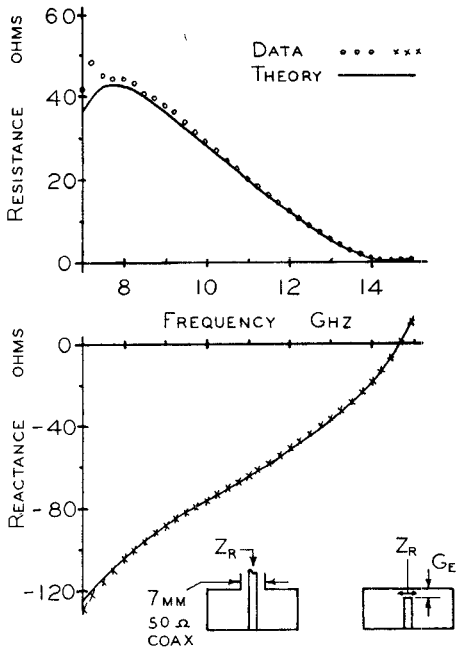

Fig. 8. Driving point impedance comparison for a coaxial entry versus an equivalent gap.

similarly for $Y_B + Y_C$ and

$$jX_L = \sum_{m=2}^{2M_1} Z_{m0}\left(\frac{\kappa_{pm}}{\kappa_{p1}}\right)^2 (1 - w') \tag{6d}$$

where Z_{G1} and Z_{G2} are the loads in the respective gaps and X_L is the post inductance [4]. The multilateral nature of this network allows independent loading on all four ports and free choice for the driving port(s). Shorting out of either gap will reduce this circuit to the single-gap circuit previously reported.

This network configuration was initially proposed by Lewin [6] when he studied the structure of Fig. 2(c). Unfortunately, his complex mathematics and the lack of experimental verification of his theory failed to establish this circuit as an accurate representation for that configuration. Now we shall see that a relatively simple set of equations describes the elements of Fig. 7, providing an equivalent circuit for the 2-gap structure with no limitations on the placement of the gaps in the post. If, however, we choose the gaps to be at the top and/or bottom of the waveguide, then any of the three configurations of Fig. 2 can be represented.

III. Experimental Verification

Before we look at the 2-gap circuit, consider briefly the equivalence mentioned between a coaxial entry and a gap located at the bottom of the waveguide. Fig. 8 demonstrates how well this equivalence holds over a very broad frequency range. The coaxial line is a 50-Ω 7-mm airline driving X-band waveguide, a commonly used combination. The results shown as plotted points are for the measured driving point impedance. This is compared to a computer calculated plot for the gap configuration with an "equivalent gap" size $G_E = 0.245$ cm. (The required equivalent gap is, as expected, a function of the characteristic impedance and coax dimensions [2].)

Utilizing this G_E, the configuration of Fig. 2(b) was considered. A standard packaged varactor diode was placed in the post gap 3.2 mm away from the wall and the coaxial input impedance was measured at two different bias conditions. These data are plotted in Fig. 9 and are compared to the theory shown. The normal

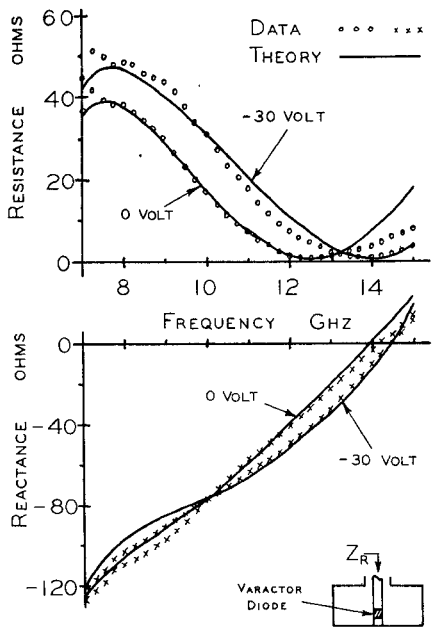

Fig. 9. Theory and experimental comparison for varactor tuning.

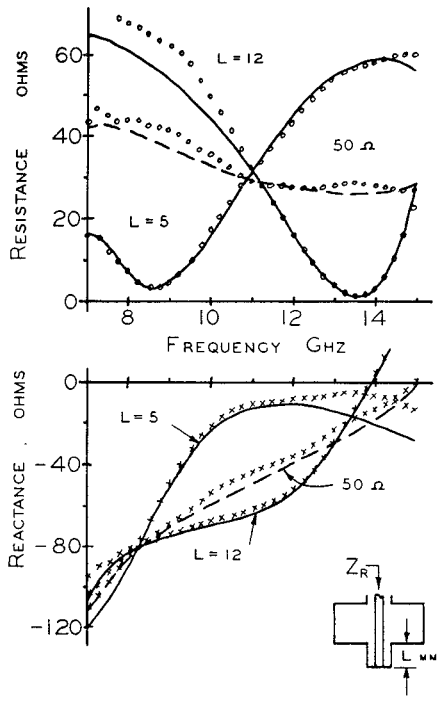

Fig. 10. Theory and experimental comparison for a 50-Ω load and a sliding short.

varactor model was used as the gap load with $L_s = 0.45$ nH, $C_p = 0.2$ pF, $R_s = 0.95\,\Omega$, $C_j(0v) = 1.9$ pF, and $C_j(-30v) = 0.45$ pF. (Note the interesting effect at midband (10 GHz) where the reactance stays constant but the real part shifts from 17 to 31 Ω. This would be more useful for amplitude modulation than for frequency tuning of a Gunn diode.)

The next mount example shown in Fig. 10 uses the double coax configuration, requiring an equivalent gap representation at both ports. Three different loading conditions are established at Z_{G2} to demonstrate the versatility of this configuration. First a 50-Ω coaxial match is used to represent a lossy load. Then two different positions of a sliding short are used to represent widely varying reactive loading. The correlation between the measured data and the theory is excellent for all three conditions. 25- and 100-Ω loads were also measured along with many other short positions. The examples shown, however, were chosen as typical and do not represent best cases.

IV. Summary and Conclusions

An equivalent circuit for a 2-gap waveguide mount has been presented. Also, an equivalence has been demonstrated between a coaxial entry and an equivalent gap for this type mount. Using this information, theoretical curves for various configurations were generated and compared with measured data. Excellent correlation was observed, indicating the accuracy of the equivalent circuit modeling for use in microwave component design.

References

[1] M. Dean and M. J. Howes, "An electronically tuned Gunn oscillator circuit," *IEEE Trans. Electron Devices*, vol. ED-20, no. 6, pp. 597–598, June 1973.
[2] R. L. Eisenhart, P. T. Greiling, L. K. Roberts, and R. Robertson, "A useful equivalence for a coaxial-waveguide junction," to be published.
[3] N. D. Kenyon, "A circuit design of millimeter-wave IMPATT oscillators," *IEEE Microwave Symposium Digest*, Newport Beach, CA, May 1970.
[4] R. L. Eisenhart and P. J. Khan, "Theoretical and experimental analysis of a waveguide mounting structure," *IEEE Trans. Microwave Theory Tech.*, vol. MTT-19, pp. 706–719, August 1971.
[5] R. E. Collin, *Foundations for Microwave Engineering.* McGraw-Hill, 1966, p. 164.
[6] L. Lewin, "A contribution to the theory of probes in waveguides," *Proc. Inst. Elec. Eng.*, Monogr. 259R, pp. 109–116, Oct. 1957.

An Improved Solid-State Noise Source

MOTOHISA KANDA

***Abstract*—An improved solid-state noise source is discussed. By implementing such modifications as 1) heat sinking of a silicon avalanche noise diode, 2) proper dc RF decoupling, and 3) impedance matching, the stability of the National Bureau of Standards (NBS) solid-state noise source is improved significantly over that of typical commercial solid-state noise sources. These modifications, how they are implemented, and the resulting improvement in stability are described.**

I. Introduction

The convenience of a high-level noise output with a potential for fast switching makes a solid-state noise source ideal for system noise monitor applications. However, solid-state noise sources are relatively easily influenced by their environment, and an unsuitable environment can cause unstable operation.

A preliminary study on the stability of typical commercial solid-state noise sources indicated that the fluctuations of the output noise for a typical commercial solid-state noise source exhibit a random walk noise behavior (which is divergent toward lower frequencies) in its average noise output. The square root of the variance of the average output noise power for a one-day sampling time interval is typically 0.008 dB [1], [2]. The low frequency divergent instability is attributed to the noise diode itself and to the external circuit in which it is used. The stability of a solid-state noise source can be improved by properly

Manuscript received March 31, 1976; revised July 22, 1976.
The author is with the Electromagnetics Division, National Bureau of Standards, Boulder, CO 80302.